Journal of the European Ceramic Society 40 (2020) 3414–3422

Contents lists available at ScienceDirect

Journal of the European Ceramic Society

journal homepage: www.elsevier.com/locate/jeurceramsoc

Original Article

In-plane thermal expansion behavior of dense ceramic matrix composites containing SiBC matrix

Xiaomeng Fan*, Xiaokang Ma[1], Xiaolin Dang, Jimei Xue, Fang Ye, Donglin Zhao, Laifei Cheng

Science and Technology on Thermostructural Composite Materials Laboratory, Northwestern Polytechnical University, Xi'an, Shaanxi, 710072, PR China

ARTICLE INFO

Keywords:
Ceramic matrix composites (CMCs)
Coefficient of thermal expansion
Thermal residual stress
Liquid silicon infiltration

ABSTRACT

In order to reveal the effect of matrix cracks resulted from thermal residual stresses (TRS) on the thermal expansion behavior of ceramic matrix composites, SiBC matrix was introduced into C_f/SiC and SiC_f/SiC by liquid silicon infiltration. The TRS in both two composites were enlarged with incorporating SiBC matrix which has higher coefficients of thermal expansion (CTEs) than SiC matrix. Due to the relatively high TRS, matrix cracks and fiber/matrix (f/m) debonding exist in C_f/SiC-SiBC, which would provide the space for the expansion of matrix with higher CTEs. For SiC_f/SiC, no matrix cracking and f/m debonding took place due to the close CTEs between fiber and matrix. Accordingly, with the incorporation of SiBC matrix, the in-plane CTE of C_f/SiC between room temperature to 1100 °C decreases from 3.65×10^{-6} to 3.19×10^{-6} K^{-1}, while the in-plane CTE of SiC_f/SiC between room temperature to 1100 °C increases slightly from 4.97×10^{-6} to 5.03×10^{-6} K^{-1}.

1. Introduction

Continuous fiber reinforced ceramic matrix composites (CMCs) have been extensively studied due to their low density, high strength at elevated temperatures and excellent thermal stability [1,2]. In their practical applications (especially the assembly with different materials), a key consideration is the thermal expansion behavior of CMCs. Coefficient of thermal expansion (CTE) is an important parameter to characterize thermal expansion behavior [3,4].

The CTE of fiber reinforced single-phase matrix composite (α_c) can be expressed by the following formula [5].

$$\alpha_c = \frac{\overline{E\alpha}}{\overline{E}} = \frac{E_f \alpha_f V_f + E_m \alpha_m V_m}{E_f V_f + E_m V_m} \quad (1)$$

where E, α and V represent the Young's modulus, CTE and volume fraction, respectively. The subscripts f and m represent the fiber and matrix, respectively. Therefore, the thermal expansion of CMCs depends on the volume fraction of fiber and matrix and their respective properties. Renz et al. [6] investigated the effect of SiC content on the thermal expansion behavior of carbon fiber reinforced dual carbon-silicon carbide matrix composite (C_f/C-SiC), and the results showed that the CTE increases as the SiC content increases. According to formula (1), when other conditions remain unchanged and only the CTE of matrix (α_m) increases, the CTE of CMC increases. On the other hand, the increase of α_m may aggravate the thermal mismatch between fiber and matrix. The most simple formula for the thermal residual stresses (TRS, σ) in CMC is as follows [7].

$$\sigma = E_m \Delta T \Delta \alpha \quad (2)$$

where ΔT is the temperature difference between operation temperature and processing temperature. $\Delta\alpha$ is the CTE difference between fiber and matrix. In effect, matrix cracking may occur, which depends on the severity of thermal mismatch degree between fiber and matrix. An important issue arises whether these matrix micro-cracks derived from TRS in turn affect the CTE of CMC.

Up to now, carbon fiber reinforced SiC matrix composite (C_f/SiC) and SiC fiber reinforced SiC matrix composite (SiC_f/SiC) fabricated by chemical vapor infiltration (CVI) are the two most widely studied CMCs [8–10]. They are also suitable material systems for studying this issue. The CTE of carbon fiber is greatly different from that of SiC matrix, leading to large TRS. While SiC fiber has a similar CTE with SiC matrix, and the TRS should be much less.

According to formula (2), the TRS in CMC can be enlarged by increasing the matrix modulus, matrix CTE or processing temperature. In our previous work, SiBC matrix was successfully introduced into C_f/SiC and SiC_f/SiC by liquid silicon infiltration (LSI) to improve the oxidation resistance, and the prepared dense C_f/SiC-SiBC and SiC_f/SiC-SiBC exhibit good oxidation resistance from 800 to 1200 °C [11,12]. First, the processing temperature of LSI (1600 °C) is higher than that of CVI

* Corresponding author.
E-mail address: fanxiaomeng@nwpu.edu.cn (X. Fan).
[1] Xiaomeng Fan and Xiaokang Ma are co-first authors; they contributed equally to the work.

https://doi.org/10.1016/j.jeurceramsoc.2020.03.006
Received 20 January 2020; Received in revised form 26 February 2020; Accepted 4 March 2020
Available online 19 March 2020
0955-2219/

(1000 °C). Second, the introduction of SiBC can improve the matrix modulus due to decreased porosity. Last, although the CTE of SiBC matrix is unknown, it should not be low due to the relatively high CTE of B_4C [13], which needs to be verified by measurements. In summary, the introduction of SiBC can enlarge the TRS in CMC. This has been proved in C_f/SiC material [14]. Multiple matrix cracks were observed in C_f/SiC-SiBC due to high TRS [11]. Therefore, the study on thermal expansion behavior of SiBC modified C_f/SiC and SiC_f/SiC is expected to reveal the effect of matrix micro-cracks on the CTE of CMC.

In this work, SiBC modified C_f/SiC and SiC_f/SiC were prepared by LSI. The thermal expansion behavior of C_f/SiC-SiBC and SiC_f/SiC-SiBC was studied systematically and compared with unmodified C_f/SiC and SiC_f/SiC. The main objective of this work is to investigate the effect of SiBC addition on the thermal expansion behavior of C_f/SiC and SiC_f/SiC and reveal its mechanism.

2. Experimental

2.1. Materials preparation

Carbon fiber (T-300, Toray, Japan) was chosen as the reinforcement, and the preform was prepared by stacking the weave fibers. The typical properties of carbon fiber are listed in Table 1. Each bundle of as-received carbon fibers contains 1000 filaments. The fiber volume fraction was 40 vol.%. After deposition of PyC interphase with a thickness of 200 nm, SiC matrix was introduced by CVI with MTS-H_2-Ar as precursors. C_f/SiC composites were obtained after the infiltration of SiC matrix for 360 h.

C_f/SiC-SiBC was obtained by a combined process as follows. First of all, after deposition of PyC interphase with a thickness of 200 nm, and the porous C_f/SiC preforms can be obtained by the infiltration of SiC matrix for 240 h. Secondly, slurry infiltration was carried out to introduce ceramic particles (B_4C) into the pores. Thirdly, liquid silicon infiltration was carried out at 1600 °C in vacuum furnace. The detailed process can be found in the previous work [14].

SiC fiber with the chemical composition of 66.5Si-33C-0.5O in mass (Nanjing Glass Fiber Institute, China) was chosen as the reinforcement, and the preform was prepared by stacking the weave fibers. The typical properties of SiC fiber are listed in Table 1. Each bundle of as-received SiC fibers contains 500 filaments. The fiber volume fraction was 28 vol.%. After deposition of BN interphase with a thickness of 500 nm, SiC_f/SiC can be obtained by the infiltration of SiC matrix for 360 h.

SiC_f/SiC-SiBC was obtained by the same combined process like C_f/SiC-SiBC, and the only difference is the deposition of BN interphase (500 nm thickness) into SiC fiber preform. The detailed information can be found in the previous work [12].

B_4C powder (D_{50} = 1.5 μm, 50 wt.%, Mudanjiang Jingangzuan Boron Carbied Co. Ltd., Mudanjiang, China) was mixed homogeneously and then pressed into bars by cold-pressing. After heat-treatment at 1400 °C for 2 h under the flowing Ar atmosphere, the green B_4C preforms were obtained. And then the infiltration of liquid silicon into B_4C green preforms was carried out to obtain SiBC ceramics.

2.2. Characterization

The specimens of 25 × 5 × 3 mm^3 was employed to test the coefficient of thermal expansion by thermal expansion instrument (DIL 402C, NETZSCH, Germany). The measurements were conducted from RT to 1100 °C in argon atmosphere with a heating rate of 5 °C/min. Tests are limited in the longitudinal direction. The length change with temperature was recorded, and CTE (α) is calculated by the following formula.

$$\alpha = (L_T - L_{T0})/L_{T0}(T - T_0) = \Delta L/L_{T0}\Delta T \quad (3)$$

Where T_0 is the reference temperature (Room temperature 25 °C); L_{T0} is the length of the samples at the reference temperature; T is the measured temperature, and L_T is the length at the measured temperature. The accuracy of the measurements is ± 3 %.

The dog-bone shape specimens were employed to do the cyclic loading-unloading tests with a loading rate of 0.1 mm/min at room temperature, which were conducted on a servo-hydraulic tester (Model 8801, Instron Ltd., High Wycombe, England). Strain gauges were glued on the opposite sides of each specimen to monitor the strains. The cyclic unloading-reloading tests were carried out with an incremental step loading of 20 MPa for per cycle up to final rupture. At least three samples were employed for each assembles.

Bulk density and open porosity of as-fabricated specimens were obtained by Archimedes' method. The microstructure of samples was characterized by scanning electron microscope (SEM, S-2700, Hitachi, Japan) and back-scattered electron image (BSE). Energy dispersive X-ray spectrum (EDS) was recorded to identify the element species. The foil sample with dimensions of 10 μm × 10 μm was prepared by the focused-ion beam technique (FIB, Helios G4 CX, FEI, USA), and then be analyzed by transmission electron microscopy (TEM, Themis Z, FEI, USA) installed with a probe aberration corrector. Sub-angstrom high-angle annular dark field (HAADF) imaging was conducted.

3. Results

3.1. Microstructure of SiBC ceramics

The density of as-obtained SiBC ceramics is 2.47 g/cm^3. As detected by XRD (Fig. 1a), the as-fabricated SiBC ceramic was composed of $B_{12}(Si,B,C)_3$, β-SiC, and silicon. The strong intensity of diffraction peak in 27° means the high crystallization degree of silicon. As shown in BSE image (Fig. 1b), the bright phase, grey phase and dark phase represent Si, SiC and $B_{12}(Si,B,C)_3$, respectively.

The SiBC foil was cut by FIB, and then the microstructure was analyzed by TEM. As shown in HAADF image (Fig. 1c), the bright phase and dark phase represent the Si and $B_{12}(Si,B,C)_3$, and minor bright phase in dark phase represent SiC, which was confirmed by the EDS mapping. It can be found that $B_{12}(Si,B,C)_3$ was formed and homogenously dispersed in the silicon matrix. As reported, the reaction of B_4C and silicon was a dissolution-precipitation process, and with the saturation of boron and carbon in silicon melt, the ternary phase $B_{12}(Si,B,C)_3$ and SiC precipitated, and the microstructure depended on the particle size of B_4C [15–18]. In this work, the employed B_4C particles have an average particle size of 1.5 μm, and all the B_4C particles were consumed completely by the excess silicon. As reported in our previous work [14], the SiBC ceramic consists of 36.7 vol.% $B_{12}(Si,B,C)_3$, 11.3 vol.% β-SiC and 52 vol.% Si.

3.2. Microstructure of CMCs containing SiBC

The apparent density and open porosity of all four composites are listed in Table 2. It can be found that the as-fabricated composites have

Table 1
Typical properties of carbon fiber and SiC fiber.

Fiber	Diameter (μm)	Density (g/cm^3)	Tensile strength (GPa)	Young's modulus (GPa)	Strain to failure (%)	Poisson's ratio
Carbon fiber	7	1.76	3.53	230	1.5	0.3
SiC fiber	12.5	3.00	3.14	310	1.12	0.2

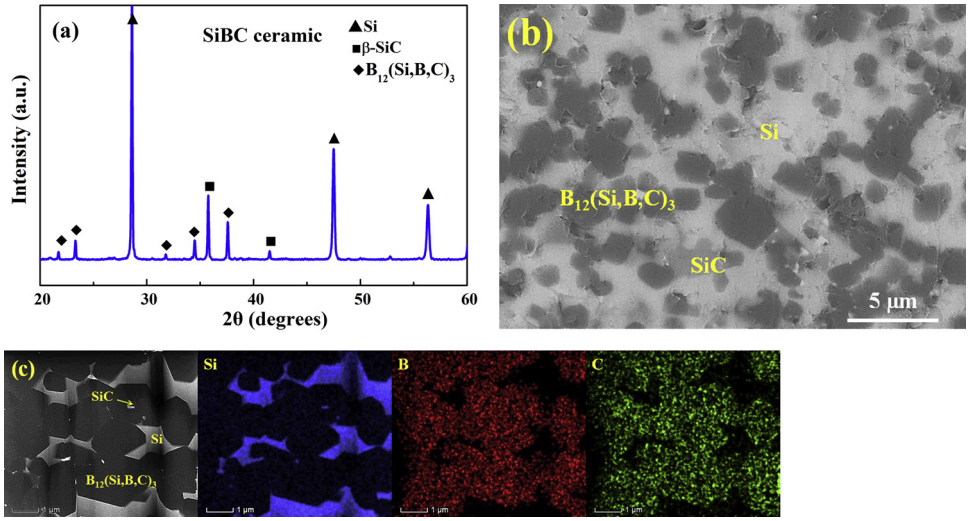

Fig. 1. (a) XRD patterns of as-fabricated samples; (b) BSE images of SiBC ceramic; (c) HAADF image and EDS mapping of SiBC ceramic.

Table 2
Density, porosity and phase composition of all four composites.

Specimen	Density (g/cm^3)	Open porosity (vol.%)	Total porosity (vol.%)	Volume content (vol.%)		
				Fiber	CVI-SiC matrix	SiBC matrix
C_f/SiC	2.11	12	16	40	44	0
C_f/SiC-SiBC	2.20	6	8	40	28	24
SiC_f/SiC	2.72	7	13	28	59	0
SiC_f/SiC-SiBC	2.57	4	11	28	28	33

lower open porosity with incorporating SiBC matrix. The high porosity of C_f/SiC and SiC_f/SiC can be attributed to the bottle-neck effect of CVI process, leading to the porous matrix. The densities of carbon fiber, SiC fiber, CVI-SiC matrix [12] are 1.76, 3.00 and 3.21 g/cm^3, and thus the SiC_f-based composites have a higher density of above 2.50 g/cm^3.

The volume fraction of CVI-SiC matrix (V_{SiC}), the volume fraction of SiBC matrix (V_{SiBC}) and the total porosity P can be calculated by the following formulas (4–5).

$$d_c = d_f \times V_f + d_{SiC} \times V_{SiC} + d_{SiBC} \times V_{SiBC} \quad (4)$$

$$P = 1\text{-}V_f\text{-}V_{SiC}\text{-}V_{SiBC} \quad (5)$$

where d_c is the measured density of composite, d_f is the density of fiber,

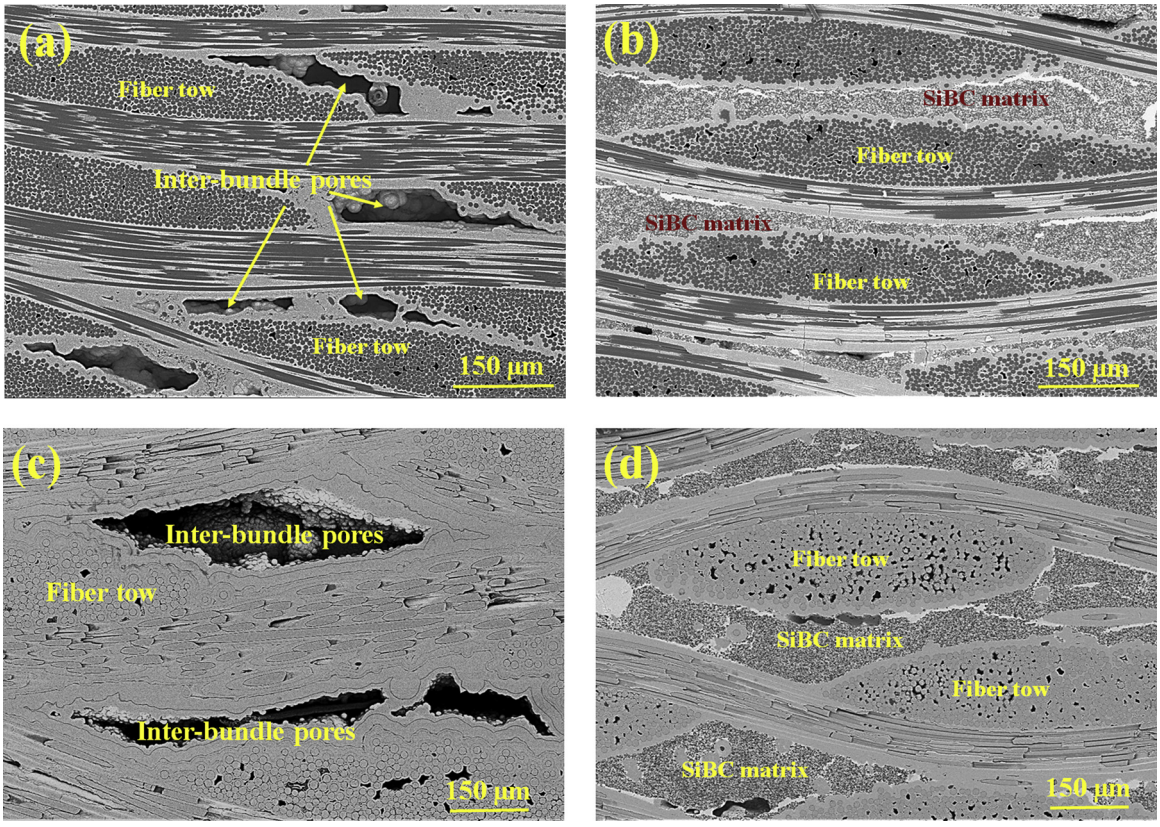

Fig. 2. BSE images of polished surface of (a) C_f/SiC, (b) C_f/SiC-SiBC, (c) SiC_f/SiC, and (d) SiC_f/SiC-SiBC.

d_{SiC} is the density of CVI-SiC matrix, d_{SiBC} is the density of SiBC matrix, V_f is the volume fraction of fiber. V_{SiBC} is 0 for C_f/SiC.

Carbon fiber preform has a high fiber volume fraction of 40 vol.%. According to Eqs. (4 and 5), the phase content can be calculated. There is 40 vol.% carbon fiber, 44 vol.% CVI-SiC matrix and 16 vol.% total porosity for C_f/SiC, and there is 40 vol.% carbon fiber, 28 vol.% CVI-SiC matrix, 24 vol.% SiBC matrix and 8 vol.% total porosity for C_f/SiC-SiBC, as listed in Table 2.

For SiC_f-based CMCs, the fiber volume fraction is 28 vol.%, and the density of SiC fiber is 3.00 g/cm^3. Using the same method according to Eqs. (4 and 5), it can be calculated that there is 28 vol.% SiC fiber, 59 vol.% CVI-SiC matrix and 13 vol.% total porosity for SiC_f/SiC, and there is 28 vol.% SiC fiber, 28 vol.% CVI-SiC matrix, 33 vol.% SiBC matrix and 11 vol.% total porosity for SiC_f/SiC-SiBC.

For 2D woven fiber perform, it can be divided into two areas, the inter-bundle and intra-bundle areas. The intra-bundle areas have a small pore size while inter-bundle areas have a large pore size. In the initial stage, the interphase and SiC matrix can deposit on fiber surface sequentially, and forming the intra-bundle microstructure. While the different inter-bundle matrix was formed due to the different process.

As shown in Fig. 2a, the pores remained in the intra-bundle and inter-bundle matrices, which is the typical microstructure characteristic for the composites fabricated by CVI. The dense inter-bundle matrix can be obtained for C_f/SiC-SiBC, which was formed by the reaction of B_4C and liquid silicon (Fig. 2b). The intra-bundle pores can be clearly seen, and the intra-bundle SiC matrix can well protect the interphase and fiber from the erosion of liquid silicon. It is also evident that the carbon fibers remain unaffected by siliconization. The fiber and interphase are surrounded by CVI-SiC matrix, and cannot be corroded by silicon.

The similar microstructure also can be found for SiC_f-based CMCs, as shown in Fig. 2c and 2d. For SiC_f/SiC composites, the inter-bundle matrix is hard to be full filled by CVI-SiC matrix, and the pores remained. While the SiBC matrix well fills the inter-bundle areas. Due to the existence of CVI-SiC matrix, the liquid silicon cannot infiltrate into the intra-bundle pores, and the intra-bundle pores remained.

3.3. Thermal expansion behavior

The expansion of SiBC and SiC matrices was measured from room temperature to 1100 °C, and the length change was recorded. Here the SiC ceramic was prepared by CVI process, and then its expansion behavior was characterized, and its CTE can be treated as the CTE of SiC matrix. As shown in Fig. 3a, it can be clearly seen that the expansion of SiBC matrix is more than that of SiC matrix in the whole temperature range. The CTEs of SiBC and SiC matrices can be calculated from the ΔL/L vs. temperature data, as shown in Fig. 3b. The CTE of CVI-SiC matrix from RT to 1100 °C is 4.9×10^{-6} K^{-1}, and that of SiBC matrix is 6.0×10^{-6} K^{-1}. As reported, the CTE of crystalline silicon from RT to 900 °C is 4.3×10^{-6} K^{-1} [19], which is lower than that of SiC.

CTEs of the composite depend on the CTEs of individual constituents, viz., fibers, SiC and SiBC matrices. The CTE of carbon fiber is anisotropic. It is reported that the axial and radial CTEs of carbon fiber are about 1.46×10^{-6} and 6.07×10^{-6} K^{-1} at 1100 °C [20], and that of employed SiC fiber is 5.1×10^{-6} K^{-1} [21]. As a summary, it can be concluded that α(carbon fiber along radius direction) > α(SiBC matrix) > α(SiC fiber) > α (SiC matrix) > α(carbon fiber along axis direction).

The linear expansion behavior of all four composites is listed in Fig. 4a. It can be found that SiC_f/SiC-SiBC shows the biggest expansion, while C_f/SiC-SiBC shows the lowest expansion in all the four composites. With incorporating SiBC matrix, the expansion of C_f/SiC decreases while that of SiC_f/SiC increases in the whole temperature range.

Fig. 4b shows the relationship between CTE and temperature of C_f/SiC and C_f/SiC-SiBC compared with SiBC and SiC matrices. The CTEs between RT to 1100 °C of C_f/SiC and C_f/SiC-SiBC are 3.65×10^{-6} and 3.19×10^{-6} K^{-1}, both of which are lower than that of SiBC and SiC matrices, resulting from the low axial CTE of carbon fiber. At the same time, with incorporating SiBC, the CTEs of C_f/SiC decrease in the whole temperature range.

The CTEs of SiC_f/SiC and SiC_f/SiC-SiBC are listed in Fig. 4c, compared with SiBC and SiC matrices. The CTEs of SiC_f/SiC and SiC_f/SiC-SiBC between RT to 1100 °C are 4.97×10^{-6} and 5.03×10^{-6} K^{-1}, both of which are close to CTE of SiC fiber (5.10×10^{-6} K^{-1}), higher than SiC matrix while lower than SiBC matrix. Both two SiC_f-based composites show the close CTE at 1100 °C, and the difference between them is only 1.21 %, which is lower than the accuracy of the measurements of CTE. As shown in Fig. 4c, it's interesting to note that the CTEs of SiC_f/SiC-SiBC in the whole temperature are higher than those of SiC_f/SiC. According to the changing tendency of CTEs, it's reasonable to say that CTEs show a slight increase with the incorporation of SiBC into SiC_f/SiC.

For SiC_f/SiC, SiC fiber has a higher CTE than SiC matrix. In the heating process, the SiC matrix would suspend the expansion of SiC fiber, leading to the lower CTE of SiC_f/SiC than SiC fiber. With the increase of testing temperature, the suspending effect was weakened, and the CTE is getting closer to SiC fiber.

As a summary, it can be concluded that α(SiC_f/SiC-SiBC) > α(SiC_f/SiC) > α(C_f/SiC) > α(C_f/SiC-SiBC). The CTEs of SiC fiber are higher than carbon fiber along axis direction, and thus SiC_f-based CMCs have higher in-plane CTEs than C_f-based CMCs. It is interesting to note that different change tendency appears for different reinforcements, the CTEs of C_f/SiC decrease but that of SiC_f/SiC increase slightly with the in-situ formation of SiBC matrix by LSI.

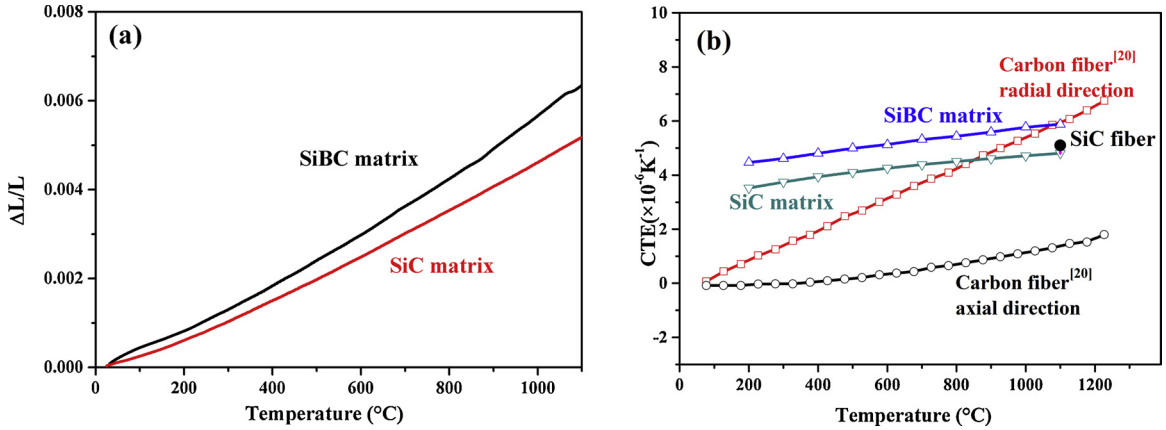

Fig. 3. (a) Relationship between in-plane linear expansion and temperature of SiBC and SiC matrices. (b) Relationship between CTE and temperature of carbon fiber [20], SiC fiber, SiC and SiBC matrices.

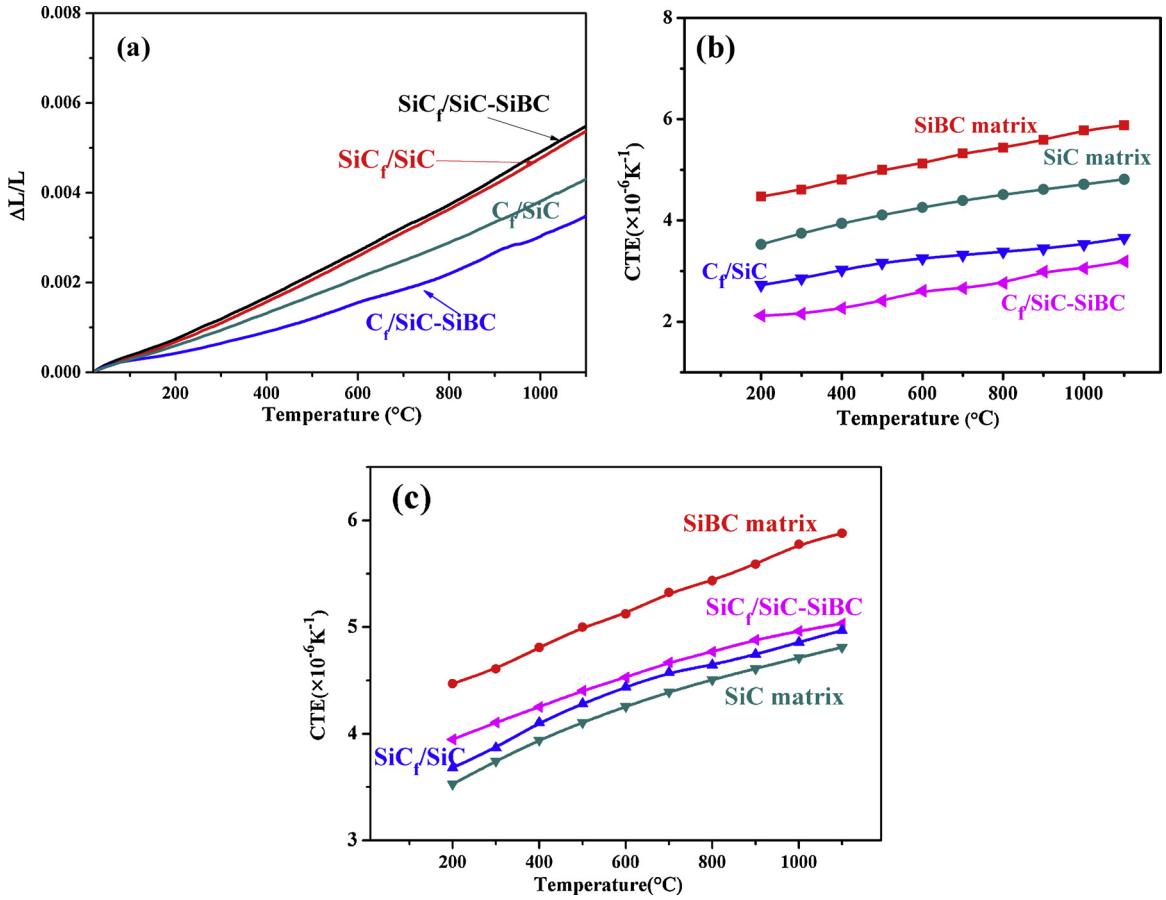

Fig. 4. (a) Relationship between in-plane linear expansion and temperature of all the four composites; Relationship between CTE and temperature of (b) C_f-based and (c) SiC_f-based CMCs compared with SiBC and SiC matrices.

3.4. Thermal residual stress

Due to the thermal mismatch between fiber and matrix, TRS always exist in the composites. Eq. (2) gave a rough estimation of the magnitude of the residual stress for the uniform composites. It can be seen as one simple method to evaluate the residual stress, and only the difference in CTE and temperature are considered, while the influences of the geometry and the elastic constants of the fiber are ignored. Actually, CMCs have non-homogenous phase distribution. The continuous fibers have orientation, especially for anisotropic carbon fiber. So, more factors should be considered, like preform woven coefficient, volume fraction of fiber, Young's modulus et al. As reported, axial TRS (σ_a) and radial TRS (σ_r) in the matrix can be estimated by the following equations [14,22]:

$$\sigma_a = E_m^* \frac{\lambda E_f V_f}{\lambda E_f V_f + E_m V_m} \times (\alpha_f^a - \alpha_m)(T_o - T_p) \quad (6)$$

$$\sigma_r = \frac{1}{(1+\nu_m)/E_m^* + (1-\nu_f)/E_f} \times (\alpha_f^r - \alpha_m)(T_o - T_p) \quad (7)$$

$$E_m^* = E_m \frac{1 - p/(1-\lambda V_f - p)}{1 + 2.5p/(1-\lambda V_f - p)} \quad (8)$$

Where V_x, ν_x, E_x refer to the volume fraction, Poisson's ratio and Young's modulus of phase x (x = f for fiber and x = m for matrix), respectively. T_o and T_p are the operation temperature and processing temperature, respectively. α_f^a, α_f^r and α_m refer to the axial CTE of fiber, radial CTE of fiber and CTE of matrix, respectively. λ is the preform woven coefficient (λ = 0.5 for 2D woven preform). E_m^* is the effective Young's modulus of matrix with pores. p is the total porosity of composite.

The Young's modulus and Poisson's ratio of carbon fiber are 230 GPa and 0.3, and those of SiC matrix are 450 GPa and 0.2 [12]. The expansion of carbon fiber is anisotropic, leading to the different stress distribution. As shown in Fig. 3b, compared with SiC matrix, the radial CTE of carbon fiber is higher, while the axial CTE of carbon fiber is lower. And thus carbon fiber is subjected to compressive stress in axial direction and tensile stress in radial direction at room temperature according to Eqs. (6 and 7). For SiC_f-based CMCs, the expansion of SiC fiber is isotropic. Due to larger CTEs of SiC fiber than SiC matrix (as shown in Fig. 3b), the SiC fiber will be under tensile stress in axial and radial direction at the room temperature according to Eqs. (6 and 7).

The typical stress-strain curves with unloading-reloading cycles of SiC_f/SiC and SiC_f/SiC-SiBC are shown in Fig. 5. Above a given applied stress, the unloading-reloading curves do not superimpose and give rise to the formation of a hysteresis loop. From the coordinates of the common intersection point by extrapolation of the compliance slopes of the top linear portion at each hysteresis loop, the axial TRS on the matrix can be obtained [23,24]. The common intersection is the origin free with thermal-residual-stress. It can be found that the intersection point locates in first quadrant of stress-strain plane for SiC_f/SiC, indicating that SiC matrix is subjected to residual compressive stress and SiC fiber is under tension, which coincides with the higher CTEs of SiC fiber than SiC matrix. While the intersection point locates in the third quadrant of stress-strain plane for SiC_f/SiC-SiBC, indicating that the SiC-SiBC matrix is subjected to residual tensile stress and SiC fiber are under compression. For SiC_f-CMCs, it can be found that α(SiBC matrix) > α(SiC fiber) > α(SiC matrix), and thus there is a transition from compressive stress to tensile stress on the matrix by incorporating SiBC matrix.

In summary, the TRS in matrix for C_f/SiC, C_f/SiC-SiBC, SiC_f/SiC and

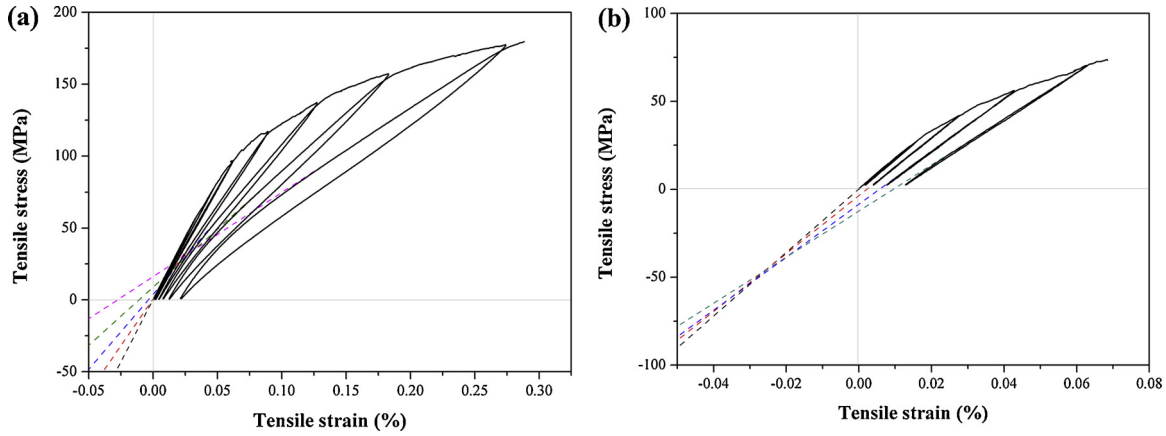

Fig. 5. Representative cyclic loading/unloading tensile curves of (a) SiC_f/SiC and (b) SiC_f/SiC-SiBC.

SiC_f/SiC-SiBC are −130 ± 34 [14], −160 ± 15 [14], 27 ± 7, −47 ± 9 MPa, respectively. The SiC matrix was prepared at 1000 °C, while the SiBC matrix was prepared at 1600 °C. The high processing temperature aggravates the CTE mismatch between fiber and matrix, leading to the higher TRS with incorporating SiBC matrix according to Eq. (6).

Except SiC_f/SiC, the matrix in other three composites is under the tensile stress. The SiC_f-CMCs show the lower value of TRS than C_f-CMCs, especially for SiC_f/SiC, the value of TRS can be as low as 27 ± 7 MPa due to the close CTE of SiC fiber and SiC matrix. With incorporating SiBC matrix, there would be tensile stress forming on the matrix, and the value of TRS increases to 47 ± 9 MPa for SiC_f/SiC-SiBC. With the replacement of SiC fiber by carbon fiber, the value of TRS increases obviously due to more serious CTE mismatch between carbon fiber and matrix.

4. Discussion

When an object is heated or cooled, its length change by an amount proportional to the original length and the change in temperature. In the testing process, the specimens were tested to heated temperature, and the length change was recorded, and then the CTE can be calculated by the linear change. The CTE of fiber reinforced single-phase matrix (α_c) can be calculated by Eq. (1). The left and right sides of Eq. (1) are divided by α_f for dimensionless, obtaining Eq. (9).

$$\frac{\alpha_c}{\alpha_f} = \frac{1}{1+E_m V_m/E_f V_f} + \frac{1}{1+E_f V_f/E_m V_m}\cdot\frac{\alpha_m}{\alpha_f} \quad (9)$$

According to Eq. (9), the relationship between the α_c and the properties of components (including modulus, CTE and volume fraction) can be depicted in Fig. 6. It can be found that, at the given constants α_f, E_m/E_f and V_m/V_f, the α_c increases as α_m increases. At the given constants α_f, α_m, E_f and V_m/V_f, the α_c increases as E_m increases under the condition of $\alpha_m > \alpha_f$, while decreases as E_m increases under the condition of $\alpha_m < \alpha_f$. It should be noted that the E_m in Eqs. (1) and (9) should take the effective modulus of matrix (E_m^*) with pores.

As reported, the Young's modulus of SiC and SiBC matrices are 450 and 305 GPa, respectively [12,14]. Using the data listed in Table 2, the E_m^* of C_f/SiC, C_f/SiC-SiBC, SiC_f/SiC and SiC_f/SiC-SiBC can be calculated to be 208, 266, 244 and 369 GPa, according to Eq. (8). It shows that, with incorporating SiBC matrix, the modulus of matrix increases. Furthermore, the CTE of matrix also increase with incorporating SiBC matrix. Hence, the CTEs of C_f-CMC and SiC_f-CMC should increase with incorporating SiBC according to Fig. 6. However, as shown in Fig. 4, with incorporating SiBC, the CTEs of C_f/SiC decrease while the CTEs of SiC_f/SiC increase slightly.

As shown in Fig. 7a, matrix cracks can be observed in C_f/SiC due to the large TRS. C_f/SiC-SiBC exhibits higher axial TRS than C_f/SiC due to the higher processing temperature and higher CTEs of SiBC matrix, leading to the more matrix microcracks in C_f/SiC-SiBC (Fig. 7b). For CVI-SiC matrix, the pores can play the role of crack pinning effect to limit the crack propagation [25]. Only cracks with small opening width can be found in inter-bundle SiC matrix. With incorporating SiBC matrix into C_f/SiC, the thermal mismatch become more serious, and the penetrated cracks can be found in the brittle SiBC matrix. At the same time, due to the larger TRS of C_f/SiC-SiBC than C_f/SiC, the cracks can penetrate into the intra-bundle matrix, as shown in Fig. 7c. It can be found that the intra-bundle crack don't be straight like the inter-bundle crack, while deflect multiple times resulting from the weak interphase.

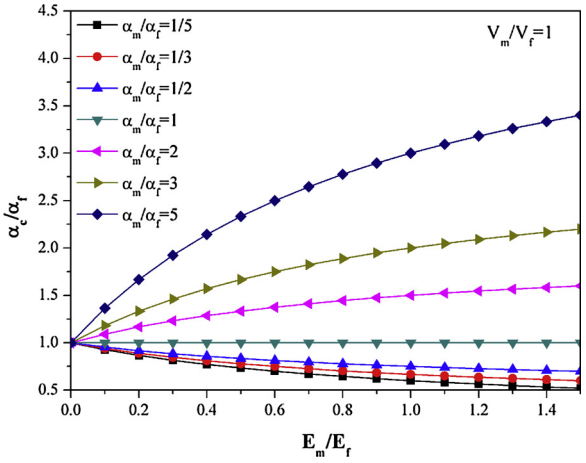

Fig. 6. Relationship between the CTE of composite and properties of components (modulus and CTE) at a constant volume ratio between matrix and fiber.

As reported [26], during pyrolysis process of manufacturing of C_f/C-SiC, the crack generation depended on the fiber-matrix interface strength, and inclined to appear in the microstructure with weak fiber/matrix strength. The similar phenomenon also can be found in the present work. As shown in Fig. 7d, when the cracks met the weak interphase, the interphase debonding took place as a result of the low interface strength.

Different from C_f/SiC, the matrix in SiC_f/SiC is under compression, so no cracks can be observed (Fig. 7e). For SiC_f/SiC-SiBC, the matrix is under tensile stress, but still no cracks can be found in the dense SiBC matrix (Fig. 7f) and no f/m debonding occurred in intra-bundle matrix (the insert of Fig. 7f), indicating that the TRS is too low to induce the crack generation.

For the present CMCs, pores and cracks exist simultaneously, and both of them would provide the space for the expansion, which may be contributed to the reduction of CTEs for C_f/SiC with the incorporation

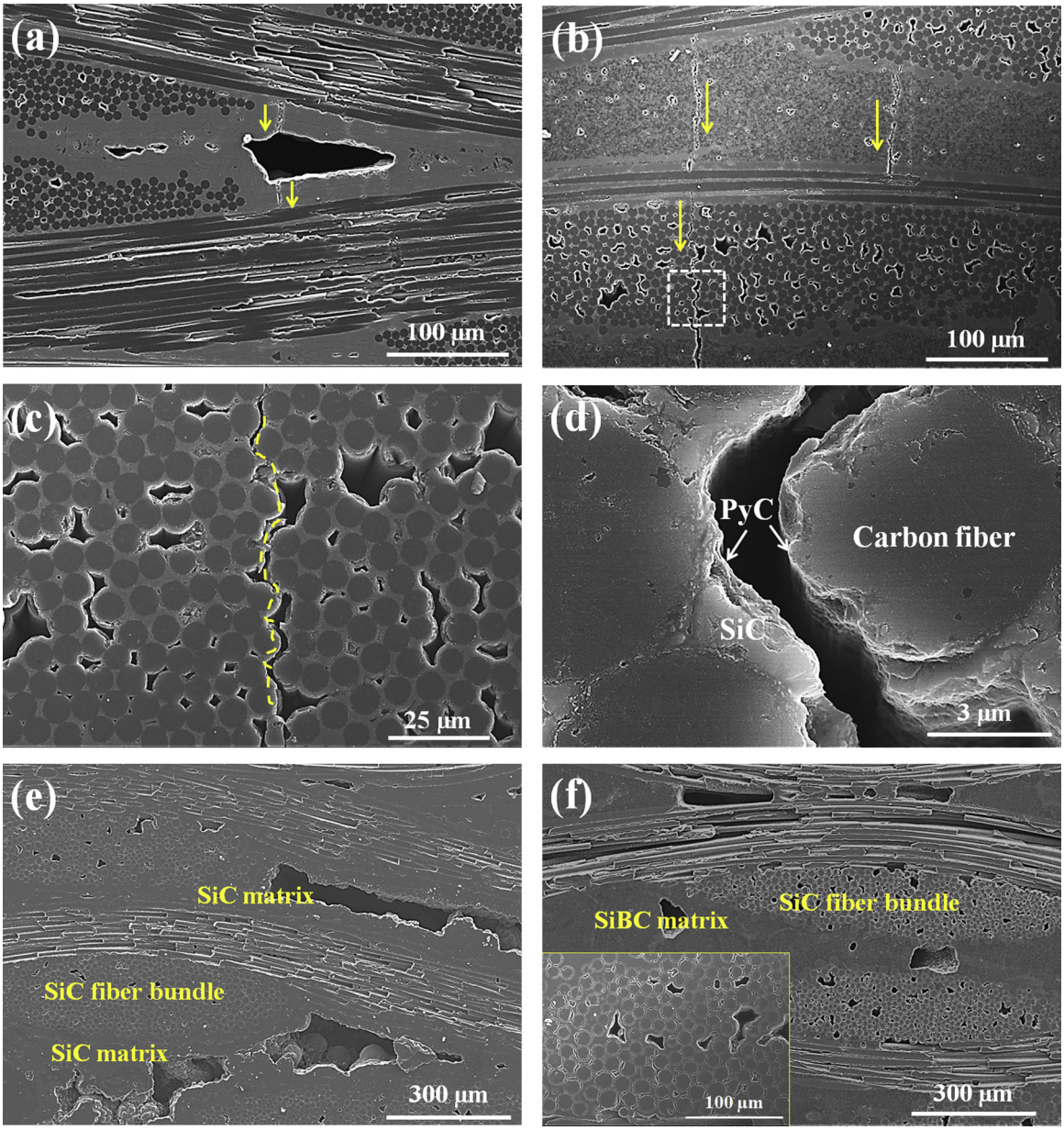

Fig. 7. SEM images of all four composites: (a) C_f/SiC, (b) C_f/SiC-SiBC, (c) matrix crack propagation and (d) f/m debonding in intra-bundle of C_f/SiC-SiBC, (e) SiC_f/SiC and (f) SiC_f/SiC-SiBC.

of SiBC matrix. Carbon fiber has lower CTE along axis direction than C_f/SiC, while SiC matrix shows higher CTE than C_f/SiC. If the matrix is composed of single SiC phase, the lower porosity means the higher Young's modulus of matrix according to Eq. (8), resulting in the higher CTEs based on the α(SiC matrix) > α(carbon fiber along axial direction), as shown in Fig. 6. From the view of carbon fiber, it was pulled by the matrix in the heating process. The lower porosity means the more matrices with high CTEs, which would lead to higher pull force and the higher CTEs.

In the present work, the lower porosity of C_f/SiC-SiBC than C_f/SiC should lead to the increase of CTEs, while the results reveal the reverse effect. As analyzed in Section 3.4, in the cooling down from processing temperature to room temperature, due to the CTE mismatch between carbon fiber and SiC matrix, the SiC matrix experienced tensile stress. If the tensile stress on the matrix is too large, the matrix cracking will take place. The thermal expansion of C_f/SiC can be treated as the reverse behavior of cooling process, and the matrix cracks would be closed gradually in the heating process. Based on the above analysis, it can be concluded that the multiple matrix cracks should be the main factor to reduce the CTEs of C_f/SiC with the incorporation of SiBC.

Based on the α(SiC fiber) > α (SiC matrix), porosity would play the oppose effect to the thermal expansion compared with C_f-based composites for SiC_f-based composites, as shown in Fig. 6, and the lower porosity leads to the decrease of CTEs. The CTEs differences between SiC_f/SiC and SiC_f/SiC-SiBC can be explained as follows. One side, SiC_f/SiC-SiBC has the lower porosity than SiC_f/SiC, which should decrease the CTEs. On the other side, the SiBC matrix has the higher CTEs than SiC fiber, which should promote the increase of CTEs. Based on the balance between these two factors, the increment of CTEs for SiC_f/SiC is not obvious with the incorporation of SiBC matrix.

Fig. 8 compares the expansion behavior of different composites and reveals the effect of matrix cracks and fiber/matrix (f/m) deboning on the CTE of composite. Fig. 8a is a composite without cracks and debonding. In such case, fiber and matrix restrict each other and keep the same expansion displacement. This expansion displacement is between the individual expansion displacements of fiber and matrix without

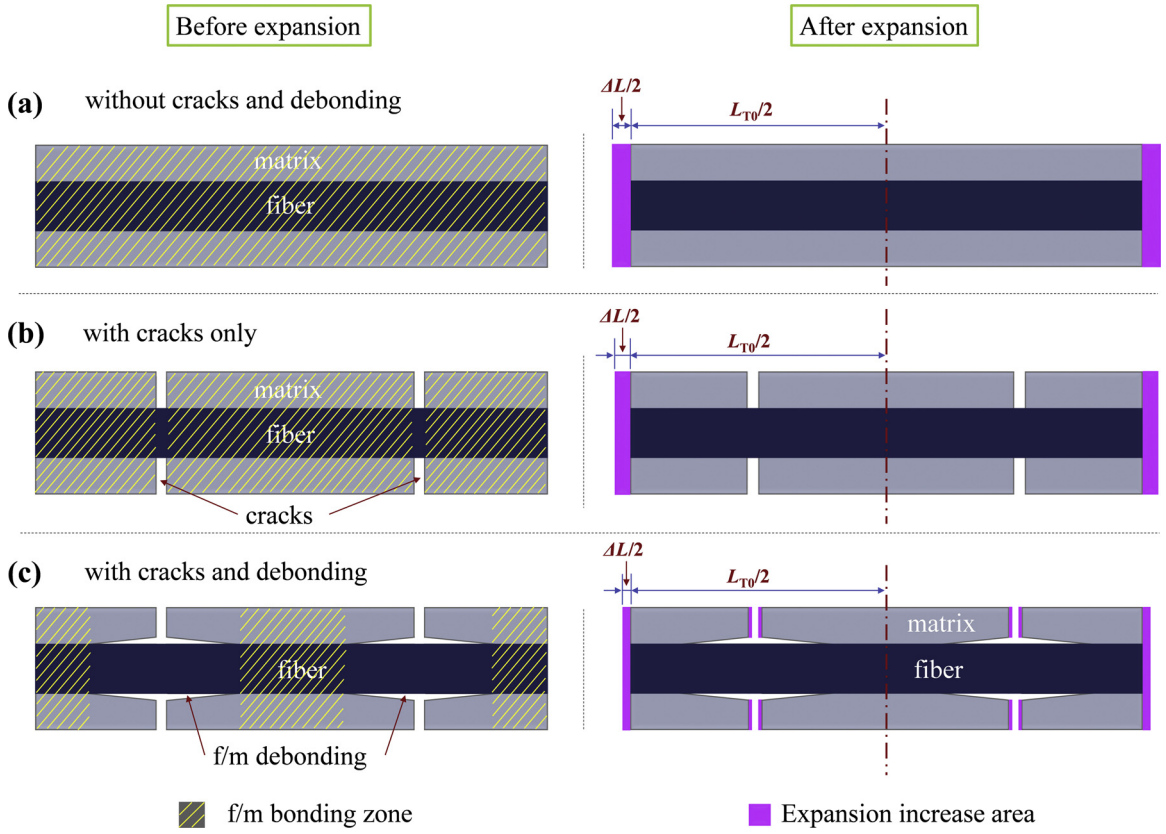

Fig. 8. Schematic diagrams of expansion behavior of composites: (a) without matrix cracks and fiber/matrix (f/m) debonding, (b) with matrix cracks only and (c) with matrix cracks and f/m debonding.

constraints based on Eq. (9). Fig. 8b is a composite with matrix cracks only. The premise of this case is: $\alpha_f^a < \alpha_m$. In such case, the fiber at crack opening is no longer constrained by the matrix. The expansion displacement of fiber at crack opening is lower than that of fiber closely bonded to matrix. Therefore, the overall ΔL in Fig. 8b is smaller than that in Fig. 8a under the same initial length L_{T0} due to the existence of matrix cracks. Actually, Fig. 8b is a hypothetical case, and matrix cracking is often accompanied by fiber/matrix (f/m) deboning due to the existence of weak interphase. Fig. 8c shows the composite with matrix cracks and f/m debonding. In such case, the fiber and matrix at f/m debonding zone are free to each other. Within a certain temperature range, the larger expansion of debonding matrix than debonding fiber is offset by crack opening. Compared with Fig. 8b, the overall ΔL in Fig. 8c decreases due to the increase of free fiber zone under the same initial length L_{T0}. Hence, the matrix cracks and f/m debonding can lower the CTE. For C_f/SiC, the incorporation of SiBC aggravates the matrix cracking (as shown in Fig. 7), leading to the decrease of CTEs. For SiC_f/SiC, there is no matrix cracks and f/m debonding, and only slight difference can be found in the CTEs between SiC_f/SiC and SiC_f/SiC-SiBC.

5. Conclusions

SiBC matrix was introduced into C_f/SiC and SiC_f/SiC composites by liquid silicon infiltration, and then the thermal expansion behavior of SiBC modified CMCs was characterized and compared with unmodified CMCs.

(1) With the introduction of SiBC matrix into C_f/SiC, the residual tensile stress on the matrix increased from 130 to 160 MPa, leading to the severe matrix cracks. With the penetration of cracks into intra-bundle matrix, the interphase debonding took place. Matrix cracks and f/m debonding can provide the space for the expansion of matrix with higher CTEs. Hence, the in-plane CTE (between room temperature to 1100 °C) decreases from 3.65×10^{-6} to $3.19 \times 10^{-6}\,K^{-1}$ when incorporating SiBC matrix into C_f/SiC.

(2) With the introduction of SiBC matrix into SiC_f/SiC, there is a transition from residual compressive stress to tensile stress on the matrix, but the low thermal residual stress cannot lead to matrix cracking. So the in-plane CTE (between room temperature to 1100 °C) increases slightly from 4.97×10^{-6} to $5.03 \times 10^{-6}\,K^{-1}$ when incorporating SiBC matrix into SiC_f/SiC.

Declaration of Competing Interest

The authors declare that they have no known competing financial interests or personal relationships that could have appeared to influence the work reported in this paper.

Acknowledgements

The authors would like to give their special thanks to Prof. Xiaowei Yin for his kind guidance and help on this research work. The authors are grateful for the support of the National Natural Science Foundation of China (Project Nos. 51725205 and 51821091), the Natural Science Foundation of Shaanxi Province (Project No. 2019JQ-634), and the Fundamental Research Funds for the Central Universities.

References

[1] X.W. Yin, L.F. Cheng, L.T. Zhang, N. Travitzky, P. Greil, Fibre-reinforced multifunctional SiC matrix composite materials, Int. Mater. Rev. 62 (2017) 117–172, https://doi.org/10.1080/09506608.2016.1213939.
[2] R.R. Naslain, The design of the fibre-matrix interfacial zone in ceramic matrix composites, Compos. Part A Appl. Sci. Manuf. 29 (1998) 1145–1155, https://doi.

org/10.1016/S1359-835X(97)00128-0.
[3] L. Cheng, Y. Xu, L. Zhang, Q. Zhang, Effect of heat treatment on the thermal expansion of 2D and 3D C/SiC composites from room temperature to 1400 ºC, Carbon 41 (2003) 1666–1670, https://doi.org/10.1016/S0008-6223(03)00125-8.
[4] S. Kumar, A. Kumar, A. Shukla, G.R. Devi, A.K. Gupta, Investigation of thermal expansion of 3D-stitched C-SiC composites, J. Eur. Ceram. Soc. 29 (2009) 2849–2855, https://doi.org/10.1016/j.jeurceramsoc.2009.04.005.
[5] R.A. Schapery, Thermal expansion coefficients of composite materials based on energy principles, J. Compos. Mater. 2 (1968) 380–404, https://doi.org/10.1177/002199836800200308.
[6] R. Renz, B. Heidenreich, W. Krenkel, A. Schöppach, F. Richter, CMC Materials for Lightweight and Low CTE Applications, High Temperature Ceramic Matrix Composites, (2001), pp. 839–845, https://doi.org/10.1002/3527605622.ch128.
[7] M. Kuntz, B. Meier, G. Grathwohl, Residual stresses in fiber-reinforced ceramics due to thermal expansion mismatch, J. Am. Ceram. Soc. 76 (1993) 2607–2612, https://doi.org/10.1111/j.1151-2916.1993.tb03988.x.
[8] R. Naslain, Design, preparation and properties of non-oxide CMCs for application in engines and nuclear reactors: an overview, Compos. Sci. Technol. 64 (2004) 155–170, https://doi.org/10.1016/S0266-3538(03)00230-6.
[9] T. Aoki, T. Ogasawara, Y. Okubo, K. Yoshida, T. Yano, Fabrication and properties of Si-Hf alloy melt-infiltrated Tyranno ZMI fiber/SiC-based matrix composites, Compos. Part A Appl. Sci. Manuf. 66 (2014) 155–162, https://doi.org/10.1016/j.compositesa.2014.07.009.
[10] T. Aoki, T. Ogasawara, Tyranno ZMI fiber/$TiSi_2$-Si matrix composites for high-temperature structural applications, Compos. Part A Appl. Sci. Manuf. 76 (2015) 102–109, https://doi.org/10.1016/j.compositesa.2015.05.018.
[11] X. Cao, X. Yin, X. Fan, L. Cheng, L. Zhang, Effect of PyC interphase thickness on mechanical behaviors of SiBC matrix modified C/SiC composites fabricated by reactive melt infiltration, Carbon 77 (2014) 886–895, https://doi.org/10.1016/j.carbon.2014.05.092.
[12] X. Sun, X. Yin, X. Fan, X. Ma, X. Cao, L. Cheng, L. Zhang, Oxidation resistance of SiC/SiC composites containing SiBC matrix fabricated by liquid silicon infiltration, J. Eur. Ceram. Soc. 38 (2) (2018) 479–485, https://doi.org/10.1016/j.jeurceramsoc.2017.09.004.
[13] C.J. Engberg, E.H. Zehms, Thermal expansion of Al_2O_3, BeO, MgO, B_4C, SiC, and TiC above 1000 ºC, J. Am. Ceram. Soc. 42 (1959) 300–305, https://doi.org/10.1111/j.1151-2916.1959.tb12958.x.
[14] X. Ma, X. Yin, X. Fan, X. Cao, L. Yang, X. Sun, L. Cheng, Improved tensile strength and toughness of dense C/SiC-SiBC with tailored PyC interphase, J. Eur. Ceram. Soc. 39 (2019) 1766–1774, https://doi.org/10.1016/j.jeurceramsoc.2019.01.006.
[15] S. Hayun, A. Weizmann, M.P. Dariel, N. Frage, Microstructural evolution during the infiltration of boron carbide with molten silicon, J. Eur. Ceram. Soc. 30 (2010) 1007–1014, https://doi.org/10.1016/j.jeurceramsoc.2009.09.021.
[16] S. Hayun, D. Rittel, N. Frage, M.P. Dariel, Static and dynamic mechanical properties of infiltrated B_4C-Si composites, Mater. Sci. Eng. A 487 (2008) 405–409, https://doi.org/10.1016/j.msea.2007.11.062.
[17] S. Hayun, N. Frage, M. Dariel, The morphology of ceramic phases in B_xC-SiC-Si infiltrated composites, J. Solid State Chem. 179 (2006) 2875–2879, https://doi.org/10.1016/j.jssc.2006.01.031.
[18] I. Solodkyi, I. Bogomol, P. Loboda, D. Batalu, A. Vlaicu, P. Badica, Floating zone partial re-melting of B_4C infiltrated with molten Si, Ceram. Inter. 43 (2017) 14718–14725, https://doi.org/10.1016/j.ceramint.2017.07.203.
[19] H. Tada, A.E. Kumpel, R.E. Lathrop, J.B. Slanina, P. Nieva, P. Zavracky, I.N. Miaoulis, P.Y. Wong, Thermal expansion coefficient of polycrystalline silicon and silicon dioxide thin films at high temperatures, J. Appl. Phys. 87 (2000) 4189–4193, https://doi.org/10.1063/1.373050.
[20] C. Pradere, C. Sauder, Transverse and longitudinal coefficient of thermal expansion of carbon fibers at high temperatures (300-2500 K), Carbon 46 (2008) 1874–1884, https://doi.org/10.1016/j.carbon.2008.07.035.
[21] R. Mo, X. Yin, F. Ye, X. Liu, X. Ma, Q. Li, L. Zhang, L. Cheng, Electromagnetic wave absorpton and mechanical properties of silicon carbide fibers reinforced silicon nitride matrix composites, J. Eur. Ceram. Soc. 39 (2019) 743–754, https://doi.org/10.1016/j.jeurceramsoc.2018.12.038.
[22] X. Ma, X. Yin, X. Fan, X. Sun, L. Yang, F. Ye, L. Cheng, Microstructure and properties of dense Tyranno-ZMI SiC/SiC containing $Ti_3Si(Al)C_2$ with plastic deformation toughening mechanism, J. Eur. Ceram. Soc. 38 (2018) 1069–1078, https://doi.org/10.1016/j.jeurceramsoc.2017.10.052.
[23] G. Camus, L. Guillaumat, S. Baste, Development of damage in a 2D woven C/SiC composite under mechanical loading: I. Mechanical characterization, Compos. Sci. Technol. 56 (1996) 1363–1372, https://doi.org/10.1016/S0266-3538(96)00094-2.
[24] G.N. Morscher, Stress-dependent matrix cracking in 2D woven SiC-fiber reinforced melt-infiltrated SiC matrix composites, Compos. Sci. Technol. 64 (2004) 1311–1319, https://doi.org/10.1016/j.compscitech.2003.10.022.
[25] Z.-Y. Deng, J. She, Y. Inagaki, J.-F. Yang, T. Ohji, Y. Tanaka, Reinforcement by crack-tip blunting in porous ceramics, J. Eur. Ceram. Soc. 24 (2004) 2055–2059, https://doi.org/10.1016/S0955-2219(03)00365-0.
[26] N. Jain, M. Kosin, Y. Shi, D. Koch, Characterization and modeling of transverse micro-cracking during pyrolysis process of carbon fiber reinforced plastics, Inter. J. Appl. Ceram. Technol. 16 (2019) 1734–1743, https://doi.org/10.1111/ijac.13312.